

The Phenomenological Research on Higgs and dark matter in the Next-to-Minimal Supersymmetric Standard Model

Zhaoxia Heng, Shenshen Yang, Xingjuan Li, Liangliang Shang^[1]

School of Physics, Henan Normal University, Xinxiang 453007, China

Abstract

The Z_3 -invariant next-to-minimal supersymmetric standard model (NMSSM) can provide a candidate for dark matter (DM). It can also be used to explain the hypothesis that the Higgs signal observed on the Large Hadron Collider (LHC) comes from the contribution of the two lightest CP-even Higgs bosons, whose masses are near 125 GeV. At present, XENON1T, LUX, and PandaX experiments have imposed very strict restrictions on direct collision cross sections of dark matter. In this paper, we consider a scenario that the observed Higgs signal is the superposition of two mass-degenerate Higgs in the Z_3 -invariant NMSSM and scan the seven-dimension parameter space composing of $\lambda, \kappa, \tan \beta, \mu, A_k, A_t, M_1$ via the Markov chain Monte Carlo (MCMC) method. We find that the DM relic density, as well as the LHC searches for sparticles, especially the DM direct detections, has provided a strong limit on the parameter space. The allowed parameter space is featured by a relatively small $\mu \leq 300$ GeV and about $\tan \beta \in (10, 20)$. In addition, the DM is Higgsino-dominated because of $|\frac{2\kappa}{\lambda}| > 1$. Moreover, the co-annihilation between $\tilde{\chi}_1^0$ and $\tilde{\chi}_1^\pm$ must be taken into account to obtain the reasonable DM relic density.

[1] e-mail: shangliangliang@htu.edu.cn (corresponding author)

I. INTRODUCTION

The 125 GeV Higgs boson was discovered in 2012 at the Large Hadron Collider (LHC) [1, 2], which has verified the validity of the standard model (SM) at energy scales around TeV. However, the existence of dark matter (DM) cannot be explained reasonably in the SM, and new physics models beyond the SM are required. The lightest supersymmetric particle (LSP) in various supersymmetric (SUSY) models provide a suitable candidate for the weakly interacting massive particle (WIMP), which is a natural prediction for DM [3–5].

The minimal supersymmetric standard model (MSSM), as one of the most popular new physics models, can provide an elegant solution to the hierarchy problem and predict the lightest neutralino as the DM candidate. Although MSSM has remarkable advantages, there are some problems, such as μ -problem and little hierarchy problem, which has been exacerbated by the LHC experiments in recent years [6–10]. These problems can be solved in the next-to-minimal supersymmetric standard model (NMSSM) extending the Higgs sector of MSSM with a gauge singlet field \hat{S} . When \hat{S} develops a vacuum expectation Value (VEV) v_s , an effective μ -term ($\mu_{eff} = \lambda v_s$) is dynamically generated, and its magnitude is naturally at the electroweak scale [11–14]. Moreover, the squared mass of SM-like Higgs boson can receive a positive contribution at tree-level because of the interactions among Higgs fields $\lambda \hat{S} \hat{H}_u \cdot \hat{H}_d$ in the NMSSM [15–19]. Furthermore, the mass can be enhanced by singlet-doublet Higgs mixing if the Higgs boson is the next-to-lightest CP-even Higgs state [20–22]. As a result, large radiative corrections to the Higgs boson mass are unnecessary and the little hierarchy problem can be avoided.

Several different methods have been proposed to diagnose whether the discovered 125 GeV Higgs boson is the superposition of two or more mass-degenerate Higgs signals [23–25]. The two-Higgs-doublet model (2HDM) [26–29] and the NMSSM [30–37] have been discussed. For example, Ref. [25] developed a method testing the presence of multiple Higgs bosons with profile likelihood techniques, which could be directly used by the ATLAS and CMS collaborations. It is known that DM direct detection experiments, such as XENON1T [38, 39], LUX [40] and PandaX [41], have imposed strict limits on DM [42, 43]. Consequently, we will scan the parameter space and explore the phenomenology considering the latest DM experiments in two mass-degenerate 125 GeV Higgs bosons of the Z_3 -invariant NMSSM. Note that we let the mass of Bino M_1 be free, which could change the composition of DM

and is different from our previous work [44].

This paper is arranged as follows: in Section II, we briefly introduce the Z_3 -invariant NMSSM and explain our scanning strategy. In Section III, we show properties of DM confronted with DM relic density and direct detection experimental results in two mass-degenerate 125 GeV Higgs bosons scenarios. In Section IV, we provide a summary.

II. MODEL AND SCAN STRATEGY

A. Basic of the Z_3 -Invariant NMSSM

The superpotential in the Z_3 -invariant NMSSM consists of the Yukawa term W_F in the MSSM and terms that are related to the additional gauge singlet chiral superfield \hat{S} :

$$W = W_F + \lambda \hat{H}_u \cdot \hat{H}_d \hat{S} + \frac{1}{3} \kappa \hat{S}^3 \quad (1)$$

where the parameters λ and κ are dimensionless and there is no μ -term in W_F . At the tree-level, the Higgs scalar potential V can be deduced from the superpotential W [11]:

$$V = V_F + V_D + V_{\text{soft}} \quad (2)$$

$$\begin{aligned} V_F &= |\lambda S|^2 (|H_u|^2 + |H_d|^2) + |\lambda H_u \cdot H_d + \kappa S^2|^2 \\ V_D &= \frac{1}{8} (g_1^2 + g_2^2) (|H_d|^2 - |H_u|^2)^2 + \frac{1}{2} g_2^2 |H_u^\dagger \cdot H_d|^2 \\ V_{\text{soft}} &= M_{H_u}^2 |H_u|^2 + M_{H_d}^2 |H_d|^2 + M_S^2 |S|^2 + (\lambda A_\lambda S H_u \cdot H_d + \frac{1}{3} \kappa A_\kappa S^3 + h.c.), \end{aligned} \quad (3)$$

where $A_{\lambda, \kappa}$ are the soft SUSY breaking trilinear parameters, and g_1 and g_2 are the gauge couplings in the $U(1)_Y$ and $SU(2)_L$ gauge symmetries. Considering the minimization conditions of the Higgs potential after electroweak symmetry breaking, $M_{H_d, H_u, S}^2$ are substituted by their vacuum expect values $\langle H_u \rangle = v_u$, $\langle H_d \rangle = v_d$ and $\langle H_s \rangle = v_s$. Then, an effective μ -term is generated as $\mu = \lambda v_s$, allowing the μ -problem in the MSSM to be solved [12]. It is known that $\mu \leq 300$ GeV is important for electroweak symmetry breaking in the NMSSM because $\mu = \lambda v_s$ and v_s should be near the electroweak scale for the singlet generally to have critical effects on electroweak phase transition [45, 46]. Finally, there are six independent parameters left in the Higgs sector of the NMSSM at the tree-level:

$$\lambda, \quad \kappa, \quad \tan \beta = \frac{v_u}{v_d}, \quad \mu, \quad A_\lambda, \quad A_\kappa \quad (4)$$

In the Z_3 -invariant NMSSM, it is convenient to use the following definition:

$$h_0 = \cos \beta H_u + \varepsilon \sin \beta H_d^*, \quad H_0 = \sin \beta H_u + \varepsilon \cos \beta H_d^* \quad (5)$$

where ε is 2-dimensional antisymmetric tensor and $\varepsilon_{12} = -\varepsilon_{21} = 1, \varepsilon_{11} = \varepsilon_{22} = 0$ [47]. Now, the $h_i = (h_0, H_0, S)^T$ can be written as

$$h_0 = \begin{pmatrix} H^+ \\ \frac{S_1 + iP_1}{\sqrt{2}} \end{pmatrix}, \quad H_0 = \begin{pmatrix} G^+ \\ v + \frac{S_2 + iG^0}{\sqrt{2}} \end{pmatrix}, \quad S = v_s + \frac{1}{\sqrt{2}}(S_3 + iP_2), \quad (6)$$

where $v^2 = v_u^2 + v_d^2$, G^+ and G^0 are the Goldstone bosons. The above equation manifests that H_0 corresponds to the Higgs field in the SM. The CP-even Higgs mass matrix in the basis (S_1, S_2, S_3) at tree-level can be described as

$$\begin{aligned} M_{S_1 S_1}^2 &= M_A^2 + (M_Z^2 - \lambda^2 v^2) \sin^2 2\beta, & M_{S_1 S_2}^2 &= -\frac{1}{2}(M_Z^2 - \lambda^2 v^2) \sin 4\beta, \\ M_{S_1 S_3}^2 &= -\left(\frac{M_A^2}{2\mu/\sin 2\beta} + \kappa v_s\right) \lambda v \cos 2\beta, & M_{S_2 S_2}^2 &= M_Z^2 \cos^2 2\beta + \lambda^2 v^2 \sin^2 2\beta, \\ M_{S_2 S_3}^2 &= 2\lambda\mu v \left[1 - \left(\frac{M_A}{2\mu/\sin 2\beta}\right)^2 - \frac{\kappa}{2\lambda} \sin 2\beta\right], \\ M_{S_3 S_3}^2 &= \frac{1}{4}\lambda^2 v^2 \left(\frac{M_A}{\mu/\sin 2\beta}\right)^2 + \kappa v_s A_\kappa + 4(\kappa v_s)^2 - \frac{1}{2}\lambda\kappa v^2 \sin 2\beta, \end{aligned}$$

where $M_A^2 = 2\mu(A_\lambda + \kappa v_s)/\sin 2\beta$. With the rotation matrix U , we can diagonalize the mass matrix M^2 and obtain the physical mass eigenstates $H_i = \sum_{j=1}^3 U_{ij} S_j$. In addition, the CP-odd mass eigenstates A_1 and A_2 can be derived in the same way. We assume $M_{H_1} < M_{H_2} < M_{H_3}$ and $M_{A_1} < M_{A_2}$. If the main component of H_i is the S_2 field, H_i is called the SM-like Higgs (denoted by h). Compared to the case in the MSSM, the mass of SM-like Higgs in the NMSSM at the tree-level could be enhanced because of the additional term $\lambda^2 v^2 \sin^2 2\beta$ and the mixing effect of (S_2, S_3) when $M_{S_3 S_3}^2 < M_{S_2 S_2}^2$. Therefore, it needs less radiative corrections in the NMSSM to obtain the 125 GeV SM-like Higgs compared with that in the MSSM [48–50]. The observable O_{if} can be used to explain that how it is possible to have multi mass-degenerate Higgs bosons under the present measurements of the Higgs boson properties at the LHC [37],

$$\begin{aligned} O_{if} &= \sum_{\alpha} O_{if}^{\alpha} \\ O_{if}^{\alpha} &= \sigma_i^{H_{\alpha}} B_f^{H_{\alpha}} \end{aligned} \quad (7)$$

where i denotes the production modes and f denotes the decay modes. The major O_{if} are listed in Table 1 in Ref. [37], of which best-fit values and uncertainties can be found in Refs. [51–55]. Note that the index α of the resonance should be summed over in Equation (7) if there are two or more mass-degenerate bosons.

The masses of charged Higgs bosons H^\pm at tree-level are given by

$$M_{H^\pm}^2 = M_A^2 + M_W^2 - \lambda^2 v^2 \quad (8)$$

The neutralinos in the NMSSM are the mixtures of the fields Bino \tilde{B}^0 , Wino \tilde{W}^0 , Higgsinos $\tilde{H}_{d,u}^0$, and Singlino \tilde{S}^0 . In the basis $\psi^0 = (-i\tilde{B}^0, -i\tilde{W}^0, \tilde{H}_d^0, \tilde{H}_u^0, \tilde{S}^0)$, one can obtain the symmetric neutralino mass matrix as

$$\mathcal{M}_0 = \begin{pmatrix} M_1 & 0 & -\frac{g_1 v_d}{\sqrt{2}} & \frac{g_1 v_u}{\sqrt{2}} & 0 \\ & M_2 & \frac{g_2 v_d}{\sqrt{2}} & -\frac{g_2 v_u}{\sqrt{2}} & 0 \\ & & 0 & -\mu & -\lambda v_u \\ & & & 0 & -\lambda v_d \\ & & & & \frac{2\kappa}{\lambda}\mu \end{pmatrix} \quad (9)$$

where M_1 and M_2 denote the gaugino soft breaking masses. With the unitary rotation matrix N , one can diagonalize the mass matrix \mathcal{M}_0 to obtain the mass eigenstates $\tilde{\chi}_i^0 = N_{ij}\psi_j^0$ ($i, j = 1, 2, 3, 4, 5$) and the mass eigenstates labeled in mass-ascending order. The lightest supersymmetric particle (LSP) $\tilde{\chi}_1^0$ can be regarded as one of the DM candidates.

Analogously, in the gauge-eigenstate basis $\psi^\pm = (\tilde{W}^+, \tilde{H}_u^+, \tilde{W}^-, \tilde{H}_d^-)$, the chargino mass matrix can be given by

$$M_{\chi^\pm} = \begin{pmatrix} 0 & X^T \\ X & 0 \end{pmatrix}, \quad X = \begin{pmatrix} M_2 & \sqrt{2}s_\beta M_W \\ \sqrt{2}c_\beta M_W & \mu \end{pmatrix} \quad (10)$$

One can obtain the mass eigenstates by two unitary rotation matrices as follows:

$$\begin{pmatrix} \chi_1^+ \\ \chi_2^+ \end{pmatrix} = U^+ \begin{pmatrix} \tilde{W}^+ \\ \tilde{H}_u^+ \end{pmatrix}, \quad \begin{pmatrix} \chi_1^- \\ \chi_2^- \end{pmatrix} = U^- \begin{pmatrix} \tilde{W}^- \\ \tilde{H}_d^- \end{pmatrix} \quad (11)$$

$$\text{diag}(M_{\chi_1^\pm}, M_{\chi_2^\pm}) = (U^+)^* X (U^-)^\dagger \quad (12)$$

B. Scan Strategies and Constraints on the Parameter Space of NMSSM

A_λ is fixed at 2 TeV because the masses of charged Higgs bosons are usually large considering the constraints from the LHC and M_{H^\pm} are determined by the parameter A_λ as shown in Equation (7). In addition, the soft breaking parameters except A_t in the slepton and squark sectors are fixed at 2 TeV because the stop trilinear coupling A_t plays an significant role in the 125 GeV Higgs boson via loop-corrected contributions. Moreover, the Wino mass M_2 is fixed at 2 TeV for simplicity because the wino-dominated DM could hardly satisfy limits from both DM and LHC experiments [22]. As a result, the Markov chain Monte Carlo (MCMC) scan is utilized in these parameters,

$$\begin{aligned} 0 < \lambda < 0.75, \quad |\kappa| < 0.75, \quad 1 < \tan \beta < 60, \quad -1 \text{ TeV} \leq M_1 \leq 1 \text{ TeV}, \\ 100 \text{ GeV} \leq \mu \leq 1 \text{ TeV}, \quad |A_\kappa| \leq 1 \text{ TeV}, \quad |A_t| \leq 5 \text{ TeV}. \end{aligned} \quad (13)$$

During the scan, we select the samples that are consistent with these constraints,

- All of the constraints are implemented in the package **NMSSMTools-5.5.3** [56, 57], which includes the Z-boson invisible decay, the LEP search for sparticles (i.e., the lower bounds on various sparticle masses and the upper bounds on the chargino/neutralino pair production rates), the B-physics observables such as the branching ratios for $B \rightarrow X_s \gamma$ and $B_s \rightarrow \mu^+ \mu^-$, and the discrepancy of the muon anomalous magnetic moment. The latest measured results are utilized for certain observables with an experimental central value, and the selected samples could explain these results at 2σ level.
- Constraints on the direct searches for Higgs bosons at LEP, Tevatron, and LHC. These constraints are implemented through the packages **HiggsSignals** [58–60] for 125 GeV Higgs data fit and **HiggsBounds** [61, 62] for non-standard Higgs boson search at colliders. Two nearly mass-degenerate CP-even Higgs bosons with masses $122 \text{ GeV} \leq M_{h_1, h_2} \leq 128 \text{ GeV}$ are required.
- The package **micrOMEGAs** [63, 64] embedded in **NMSSMTools** is utilized to calculate the thermally averaged cross section, the DM relic density, and the spin-dependent (SD) and spin-independent (SI) DM-nucleon cross sections of DM. The LSP $\tilde{\chi}_1^0$ should be with a thermal abundance matching the observed DM density. What's more, DM

could be composed of a lightest neutralino, an axion [65] or gravitino [66], so that we suppose that there was a large amount of DM in the early universe, and they reached the current Planck observation $\Omega_{\text{DM}}h^2 = 0.120 \pm 0.01$ as they freezed out [67–69]. Consequently, the DM relic density is required to be less than the central value 0.12 in our work. In addition to the relic density, the DM should be compatible with direct detection rates in accordance with current limits, which come from LUX-2017 [40], XENON1T-2019 [39] for SD cross sections, and XENON1T-2018 [38] for SI cross sections. It is noticed that the DM-nucleon cross sections should be scaled by a factor $\Omega h^2/0.120$ given that the LSP $\tilde{\chi}_1^0$ is only one of the DM candidates.

- Results from LHC searching sparticles. Processes $pp \rightarrow \tilde{\chi}_1^\pm \tilde{\chi}_1^0$, $pp \rightarrow \tilde{\chi}_1^\pm \tilde{\chi}_2^0$ and $pp \rightarrow \tilde{\chi}_1^+ \tilde{\chi}_1^-$ are put into Prospino2 [70] to calculate their NLO cross sections at LHC 13 TeV. Then, these processes and cross sections are fed into SModelS-2.1.1 [71], which decomposes spectrums and converts them into simplified model topologies to compare with the results interpreted from the LHC.

III. PROPERTIES OF DM

We calculate the SI and SD cross sections for samples satisfying the constraints listed in Section II. Additionally, we project these samples in the plane of $\sigma_p^{SI} - \sigma_n^{SD}$ in Figure 1, where gray samples are excluded by the SI detection coming from XENON1T-2018 [38], XENON1T-2019 [39], pink samples are excluded by the SD detection coming from LUX-2017 [40], and orange (green) samples are consistent with (excluded by) both the SD and SI detections. From this figure, we find that the DM direct detections impose a strong constraint on the parameter space in the scenario of two mass-degenerate Higgs bosons in the Z_3 -invariant NMSSM, and the constraints from direct and indirect detections of DM are complementary.

We project the samples on the left plane of $\lambda - 2\kappa$ and right plane of $|M_{\tilde{\chi}_1^\pm} - M_{\tilde{\chi}_1^0}| - M_{\tilde{\chi}_1^\pm}$ in Figure 2. From the left plane, we can see that most of the surviving samples fall within the range of $|\frac{2\kappa}{\lambda}| > 1$, which leads to decoupling Singlino in DM composition, as shown in Equation (9). From the right plane, we can see that samples with large mass differences between $\tilde{\chi}_1^0$ and $\tilde{\chi}_1^\pm$ are almost ruled out by DM direct detections because the co-annihilation between $\tilde{\chi}_1^0$ and $\tilde{\chi}_1^\pm$ must be taken into account to obtain the reasonable DM relic density.

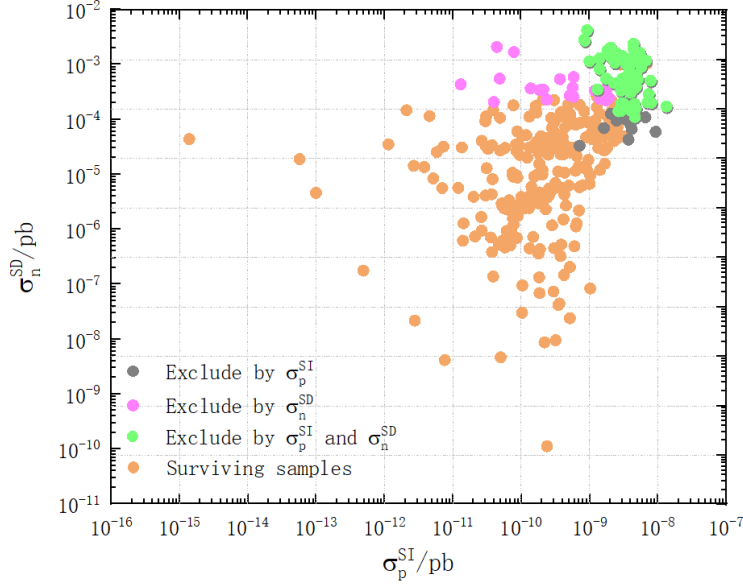


FIG. 1: Spin-dependent (SD) and spin-independent (SI) cross sections for samples satisfying the constraints listed in Section II. The limitation comes from LUX-2017 [40], XENON1T-2019 [39] for SD cross sections, and XENON1T-2018 [38] for SI cross sections.

Masses of $\tilde{\chi}_1^0$ and $\tilde{\chi}_1^\pm$ are nearly close to each other within 10% in the range from about 96 GeV to 240 GeV. In addition, we find that samples being consistent with DM direct detections are featured by a relatively small $\mu \leq 300$ GeV, with the value of $\tan\beta$ between about 10 and 20.

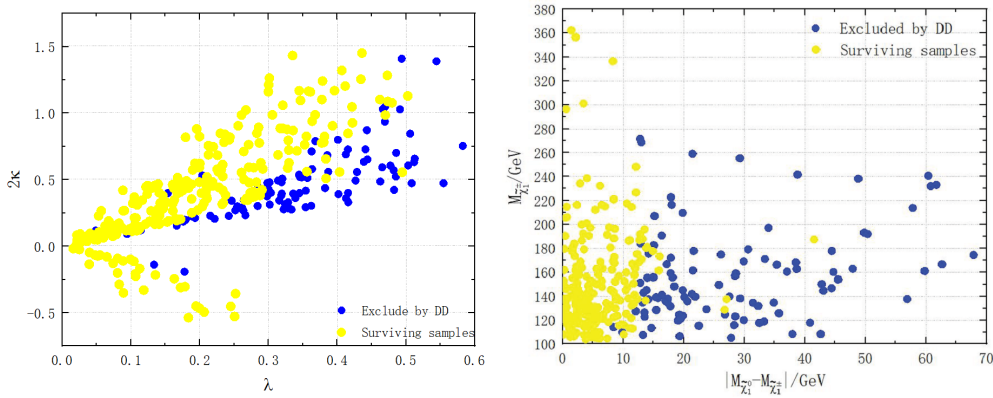


FIG. 2: Samples projected on the left plane of $\lambda - 2\kappa$ and right plane of $|M_{\tilde{\chi}_1^\pm} - M_{\tilde{\chi}_1^0}| - M_{\tilde{\chi}_1^\pm}$. Blue samples are excluded by the DM direct detections but yellow samples are consistent with these detections.

We show compositions of $\tilde{\chi}_1^0$, $\tilde{\chi}_2^0$, and $\tilde{\chi}_3^0$ for samples being consistent with DM direct detections Figure 3. From this figure, we can see that $\tilde{\chi}_1^0$ and $\tilde{\chi}_2^0$ are Higgsino-dominated, and \tilde{H}_d^0 and \tilde{H}_u^0 components are comparable; however, $\tilde{\chi}_3^0$ is Singlino-dominated.

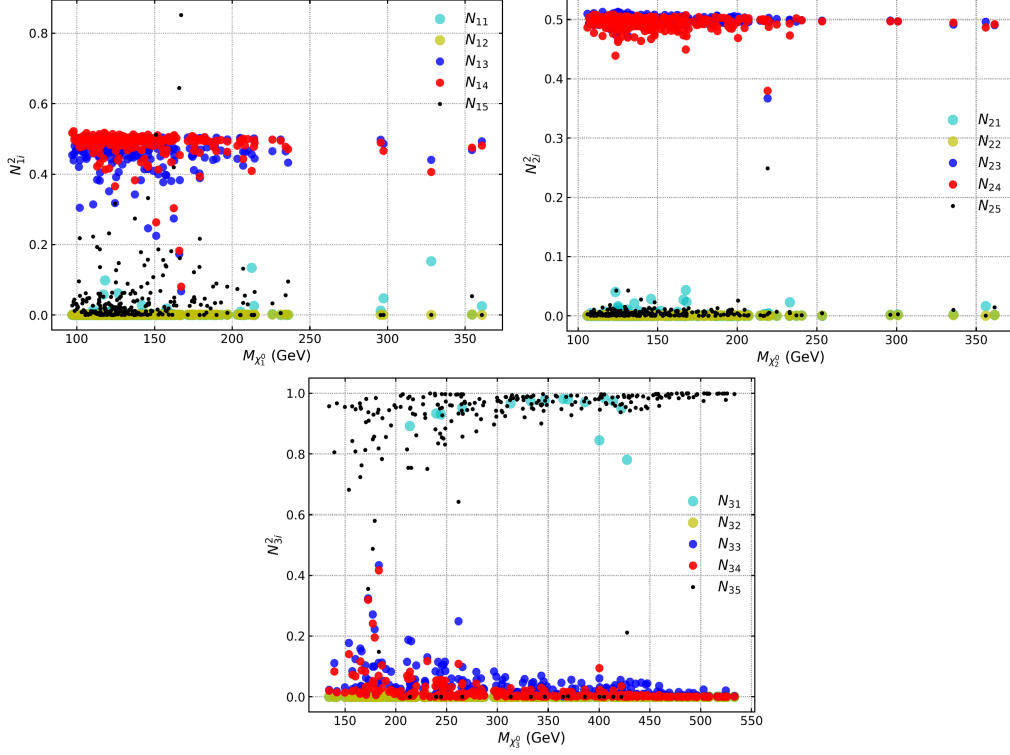


FIG. 3: Compositions of $\tilde{\chi}_1^0$, $\tilde{\chi}_2^0$, and $\tilde{\chi}_3^0$ for samples being consistent with DM direct detections.

We show contributions to DM relic density for annihilation and co-annihilation modes for samples being consistent with DM direct detections in Figure 4. The primary annihilation channel is $\tilde{\chi}_1^0 \tilde{\chi}_1^0 \rightarrow W^+ W^-$, as shown in the first row, of which tree-level Feynman diagrams are shown in the first row in Figure 5. Its distribution is approximately triangular with few zero points. The LSP mass ranges from about 97 GeV to 361 GeV, of which contributions are about 29.1% and 2.44%, respectively. The largest contribution is about 48.0% at $M_{\tilde{\chi}_1^0} = 102$ GeV, and the smallest contribution is about 1.11% at $M_{\tilde{\chi}_1^0} = 124$ GeV.

The sub-dominant annihilation channel is $\tilde{\chi}_1^0 \tilde{\chi}_1^0 \rightarrow ZZ$, as shown in the first row. Its distribution resembles that of the primary annihilation with the exception of a lower peak. The largest contribution is about 29.5% at $M_{\tilde{\chi}_1^0} = 145$ GeV. However, the annihilation channel $\tilde{\chi}_1^0 \tilde{\chi}_1^0 \rightarrow t\bar{t}$ in the second row is not as important as those we just mentioned above. Its contribution is sparse, with many zero percents, and ranges from about 1.21% to 66.0%.

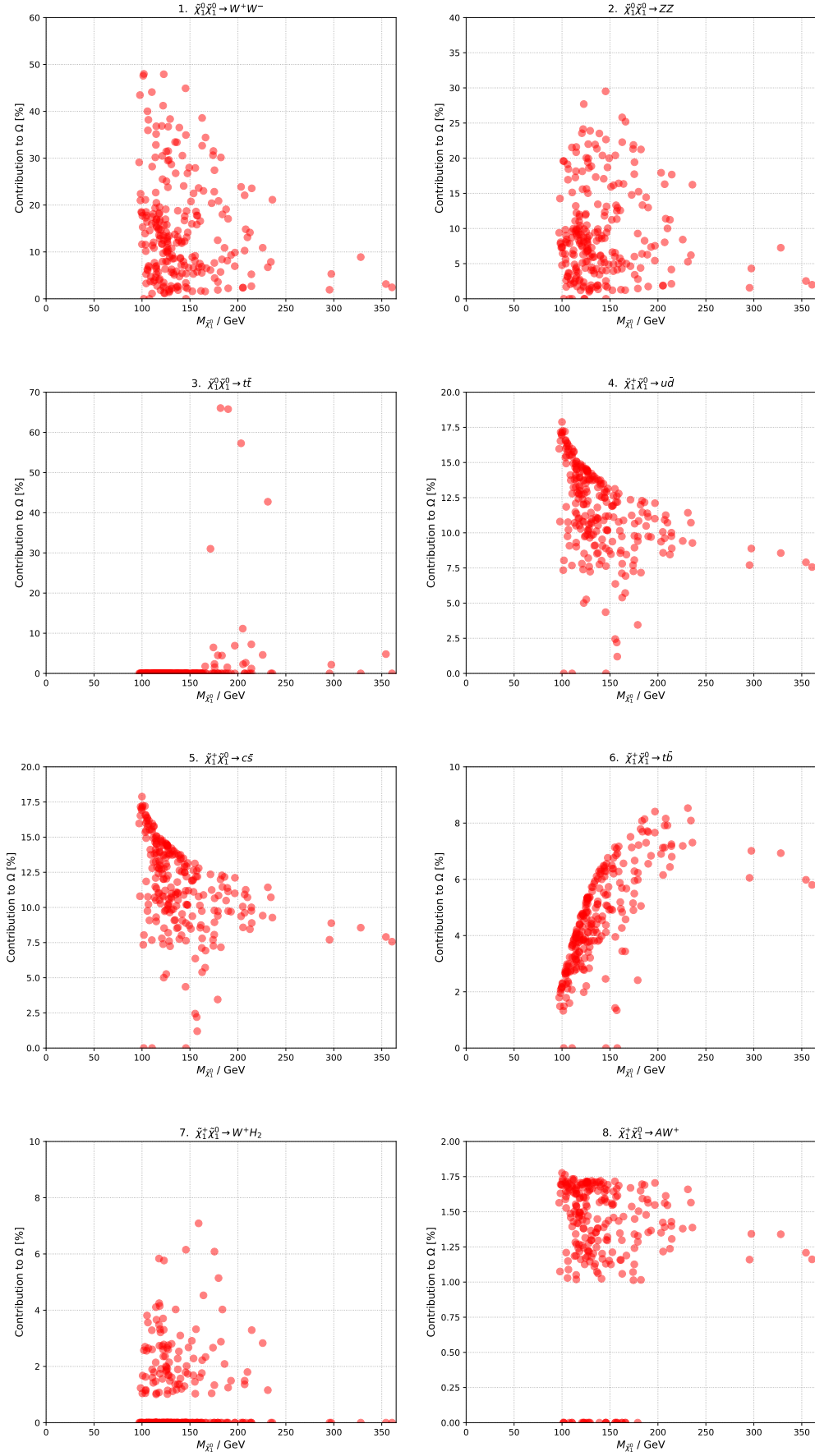


FIG. 4: Contributions of annihilation and co-annihilation processes to DM relic density for sam-

The co-annihilation between $\tilde{\chi}_1^0$ and $\tilde{\chi}_1^\pm$ must be taken into account to obtain the reasonable DM relic density. The primary channels in the co-annihilation mode are $\tilde{\chi}_1^+ \tilde{\chi}_1^0 \rightarrow u \bar{d}$ and $\tilde{\chi}_1^+ \tilde{\chi}_1^0 \rightarrow c \bar{s}$, as shown in the second row and the third row in Figure 4, respectively. The tree-level Feynman diagrams for $\tilde{\chi}_1^+ \tilde{\chi}_1^0 \rightarrow u \bar{d}$ are shown in the second row in Figure 5. The LSP mass ranges from about 97 GeV to 361 GeV for both channels, of which contributions are about 16.0% and 7.56%, respectively, but the majority of the samples are located at about $M_{\tilde{\chi}_1^0} \in [97, 236]$ GeV with contribution percents [16.0, 9.23]%. In addition, the largest contribution is 17.9% at $M_{\tilde{\chi}_1^0} = 100$ GeV, and the smallest contribution is 1.20% at $M_{\tilde{\chi}_1^0} = 156$ GeV. The sub-dominant co-annihilation channels are $\tilde{\chi}_1^+ \tilde{\chi}_1^0 \rightarrow t \bar{b}$

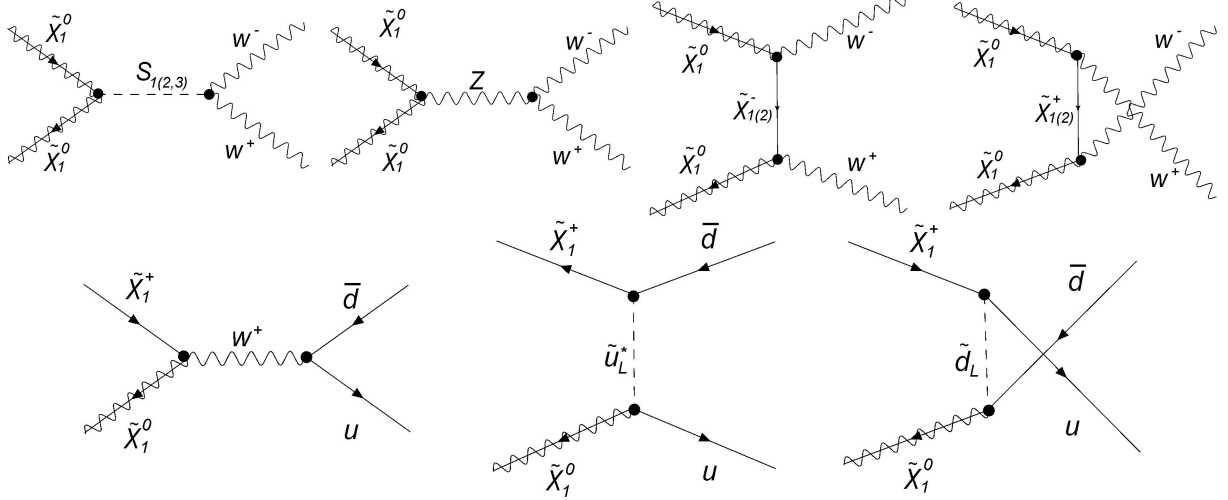


FIG. 5: Typical tree-level diagrams contributing to DM annihilation in the first row and co-annihilation in the second row.

and $\tilde{\chi}_1^+ \tilde{\chi}_1^0 \rightarrow W^+ h_2$, as shown in the third row and the last row in Figure 4. The distribution of $\tilde{\chi}_1^+ \tilde{\chi}_1^0 \rightarrow t \bar{b}$ shows an opposite trend compared to that of $\tilde{\chi}_1^+ \tilde{\chi}_1^0 \rightarrow u \bar{d}$ or $\tilde{\chi}_1^+ \tilde{\chi}_1^0 \rightarrow c \bar{s}$ in the region $M_{\tilde{\chi}_1^0} \in [100, 150]$ GeV. The largest contribution for $\tilde{\chi}_1^+ \tilde{\chi}_1^0 \rightarrow t \bar{b}$ is about 8.53% at $M_{\tilde{\chi}_1^0} = 231$ GeV. The largest contribution for $\tilde{\chi}_1^+ \tilde{\chi}_1^0 \rightarrow W^+ h_2$ is about 7.09% at $M_{\tilde{\chi}_1^0} = 159$ GeV. Finally, the last co-annihilation channel is $\tilde{\chi}_1^+ \tilde{\chi}_1^0 \rightarrow A W^+$, as shown in the last row in Figure 4, of which contributions do not exceed 2.0%.

In conclusion, we find that the LSP annihilation makes a contribution to the DM relic density in the allowed parameter space, but its contribution is insufficient to obtain the proper density. To achieve the observed value, the major LSP co-annihilation with $\tilde{\chi}_1^\pm$ should be considered.

IV. SUMMARY

In this paper, we study the property of the allowed parameter space in the Z_3 -invariant-NMSSM. We consider two mass-degenerate Higgs bosons as the observed 125 GeV Higgs, LHC searches for sparticles, the DM relic density, and the DM direct detections. These detections come from LUX-2017 and XENON1T-2019 for the SD cross sections, and XENON1T-2018 for the SI cross sections. We perform the MCMC scan over the seven-dimension parameter space composed of $\lambda, \kappa, \tan \beta, \mu, A_k, A_t, M_1$.

Our study indicates that there are still samples capable of predicting the observed 125 GeV Higgs in the case of two mass-degenerate neutral CP-even Higgs bosons in the Z_3 -invariant-NMSSM. However, the DM relic density, and the LHC searches for sparticles, especially the DM direct detections, have provided a strong limit on the parameter space. The allowed parameter space is featured by a relatively small $\mu \leq 300$ GeV and about $\tan \beta \in (10, 20)$. In addition, the DM is Higgsino-dominated because of $|\frac{2\kappa}{\lambda}| > 1$. Moreover, the co-annihilation between $\tilde{\chi}_1^0$ and $\tilde{\chi}_1^\pm$ must be taken into account to obtain the reasonable DM relic density. What is more, it is noticed that our work indicates that SUSY processes with degenerate masses of $\tilde{\chi}_1^0$ and $\tilde{\chi}_1^\pm$ within 10% in the range from approximately 96 GeV to 240 GeV can be made at LHC Run 3 or HL-LHC to validate or disprove our model's assumptions.

Acknowledgments

We thank Junjie Cao for helpful discussions. This work is supported by the National Research Project Cultivation Foundation of Henan Normal University under Grant No. 2021PL10 and powered by the High-Performance Computing Center of Henan Normal University.

-
- [1] Aad, G.; Abajyan, T.; Abbott, B.; Abdallah, J.; Khalek, S.A.; Abdelalim, A.A.; Aben, R.; Abi, B.; Abolins, M.; AbouZeid, O.S.; et al. Observation of a new particle in the search for the Standard Model Higgs boson with the ATLAS detector at the LHC. *Phys. Lett. B* **2012**, *716*, 1–29. [CrossRef]

- [2] Chatrchyan, S.; Khachatryan, V.; Sirunyan, A.M.; Tumasyan, A.; Adam, W.; Aguilo, E.; Bergauer, T.; Dragicevic, M.; Erö, J.; Fabjan, C.; et al. Observation of a New Boson at a Mass of 125 GeV with the CMS Experiment at the LHC. *Phys. Lett. B* **2012**, *716*, 30–61. [CrossRef]
- [3] Jungman, G.; Kamionkowski, M.; Griest, K. Supersymmetric dark matter. *Phys. Rept.* **1996**, *267*, 195–373. [CrossRef]
- [4] Cao, J.; Lian, J.; Pan, Y.; Yue, Y.; Zhang, D. Impact of recent $(g - 2)_\mu$ measurement on the light CP-even Higgs scenario in general Next-to-minimal supersymmetric standard model. *JHEP* **2022**, *3*, 203. [CrossRef]
- [5] Han, T.; Liu, Z.; Su, S. Light Neutralino dark matter: Direct/Indirect Detection and Collider Searches. *JHEP* **2014**, *8*, 93. [CrossRef]
- [6] Randall, L.; Sundrum, R. Out of this world supersymmetry breaking. *Nucl. Phys. B* **1999**, *557*, 79–118. [CrossRef]
- [7] Gherghetta, T.; Pomarol, A. The Standard model partly supersymmetric. *Phys. Rev. D* **2003**, *67*, 085018. [CrossRef]
- [8] Wang, F.; Wang, W.; Yang, J.M.; Zhou, S. Singlet extension of the MSSM as a solution to the small cosmological scale anomalies. *Phys. Rev. D* **2014**, *90*, 035028. [CrossRef]
- [9] Wang, F.; Wang, W.; Yang, J.; Zhang, Y.; Zhu, B. Low Energy Supersymmetry Confronted with Current Experiments: An Overview. *Universe* **2022**, *8*, 178. [CrossRef]
- [10] Harz, J.; Herrmann, B.; Klasen, M.; Kovarik, K.; Steppeler, P. Precise Prediction of the dark matter Relic Density within the MSSM. In Proceedings of the European Physical Society Conference on High Energy Physics (EPS-HEP2015), Vienna, Austria, 22–29 July 2015.
- [11] Ellwanger, U.; Hugonie, C.; Teixeira, A.M. The Next-to-minimal supersymmetric standard model. *Phys. Rept.* **2010**, *496*, 1–77. [CrossRef]
- [12] Maniatis, M. The Next-to-Minimal Supersymmetric extension of the Standard Model reviewed. *Int. J. Mod. Phys. A* **2010**, *25*, 3505–3602. [CrossRef]
- [13] Cao, J.; Ding, F.; Han, C.; Yang, J.M.; Zhu, J. A light Higgs scalar in the NMSSM confronted with the latest LHC Higgs data. *JHEP* **2013**, *11*, 18. [CrossRef]
- [14] Cao, J.; Guo, X.; He, Y.; Wu, P.; Zhang, Y. Diphoton signal of the light Higgs boson in natural NMSSM. *Phys. Rev. D* **2017**, *95*, 116001. [CrossRef]
- [15] Ellwanger, U. A Higgs boson near 125 GeV with enhanced di-photon signal in the NMSSM.

- JHEP* **2012**, *3*, 44. [CrossRef]
- [16] Gunion, J.F.; Jiang, Y.; Kraml, S. The Constrained NMSSM and Higgs near 125 GeV. *Phys. Lett. B* **2012**, *710*, 454–459. [CrossRef]
 - [17] Kang, Z.; Li, J.; Li, T. On Naturalness of the MSSM and NMSSM. *JHEP* **2012**, *11*, 24. [CrossRef]
 - [18] King, S.F.; Muhlleitner, M.; Nevzorov, R. NMSSM Higgs Benchmarks Near 125 GeV. *Nucl. Phys. B* **2012**, *860*, 207–244. [CrossRef]
 - [19] Cao, J.-J.; Heng, Z.-X.; Yang, J.-M.; Zhang, Y.-M.; Zhu, J.-Y. A SM-like Higgs near 125 GeV in low energy SUSY: A comparative study for MSSM and NMSSM. *JHEP* **2012**, *3*, 86. [CrossRef]
 - [20] Cao, J.; He, Y.; Shang, L.; Zhang, Y.; Zhu, P. Current status of a natural NMSSM in light of LHC 13 TeV data and XENON-1T results. *Phys. Rev. D* **2019**, *99*, 075020. [CrossRef]
 - [21] Cao, J.; He, Y.; Shang, L.; Su, W.; Wu, P.; Zhang, Y. Strong constraints of LUX-2016 results on the natural NMSSM. *JHEP* **2016**, *10*, 136. [CrossRef]
 - [22] Cao, J.; He, Y.; Shang, L.; Su, W.; Zhang, Y. Natural NMSSM after LHC Run I and the Higgsino dominated dark matter scenario. *JHEP* **2016**, *8*, 37. [CrossRef]
 - [23] Gunion, J.F.; Jiang, Y.; Kraml, S. Diagnosing Degenerate Higgs Bosons at 125 GeV. *Phys. Rev. Lett.* **2013**, *110*, 051801. [CrossRef] [PubMed]
 - [24] Grossman, Y.; Surujon, Z.; Zupan, J. How to test for mass degenerate Higgs resonances. *JHEP* **2013**, *3*, 176. [CrossRef]
 - [25] David, A.; Heikkilä, J.; Petrucciani, G. Searching for degenerate Higgs bosons: A profile likelihood ratio method to test for mass-degenerate states in the presence of incomplete data and uncertainties. *Eur. Phys. J. C* **2015**, *75*, 49. [CrossRef]
 - [26] Han, X.-F.; Wang, L.; Yang, J.M. Higgs pair signal enhanced in the 2HDM with two degenerate 125 GeV Higgs bosons. *Mod. Phys. Lett. A* **2016**, *31*, 1650178. [CrossRef]
 - [27] Bian, L.; Chen, N.; Su, W.; Wu, Y.; Zhang, Y. Future prospects of mass-degenerate Higgs bosons in the CP -conserving two-Higgs-doublet model. *Phys. Rev. D* **2018**, *97*, 115007. [CrossRef]
 - [28] Han, X.-F.; Wang, L.; Zhang, Y. dark matter, electroweak phase transition, and gravitational waves in the type II two-Higgs-doublet model with a singlet scalar field. *Phys. Rev. D* **2021**, *103*, 035012. [CrossRef]

- [29] Han, X.-F.; Wang, F.; Wang, L.; Yang, J.M.; Zhang, Y. Joint explanation of W-mass and muon $g-2$ in the 2HDM. *Chin. Phys. C* **2022**, *46*, 103105. [CrossRef]
- [30] Gunion, J.F.; Jiang, Y.; Kraml, S. Could two NMSSM Higgs bosons be present near 125 GeV? *Phys. Rev. D* **2012**, *86*, 071702. [CrossRef]
- [31] Munir, S.; Roszkowski, L.; Trojanowski, S. Simultaneous enhancement in $\gamma\gamma, b\bar{b}$ and $\tau^+\tau^-$ rates in the NMSSM with nearly degenerate scalar and pseudoscalar Higgs bosons. *Phys. Rev. D* **2013**, *88*, 055017. [CrossRef]
- [32] AbdusSalam, S.; Cabrera, M.E. Revealing mass-degenerate states in Higgs boson signals. *Eur. Phys. J. C* **2019**, *79*, 1034. [CrossRef]
- [33] Moretti, S.; Munir, S. Two Higgs Bosons near 125 GeV in the Complex NMSSM and the LHC Run I Data. *Adv. High Energy Phys.* **2015**, *2015*, 509847. [CrossRef]
- [34] Wang, F.; Wang, W.; Wu, L.; Yang, J.M.; Zhang, M. Probing degenerate heavy Higgs bosons in NMSSM with vector-like particles. *Int. J. Mod. Phys. A* **2017**, *32*, 1745005. [CrossRef]
- [35] AbdusSalam, S. Testing Higgs boson scenarios in the phenomenological NMSSM. *Eur. Phys. J. C* **2019**, *79*, 442. [CrossRef]
- [36] Das, B.; Moretti, S.; Munir, S.; Poulou, P. Two Higgs bosons near 125 GeV in the NMSSM: beyond the narrow width approximation. *Eur. Phys. J. C* **2017**, *77*, 544. [CrossRef]
- [37] Shang, L.; Zhang, X.; Heng, Z. The mass-degenerate SM-like Higgs and anomaly of $(g-2)_\mu$ in μ -term extended NMSSM. *JHEP* **2022**, *8*, 147. [CrossRef]
- [38] Aprile, E.; Aalbers, J.; Agostini, F.; Alfonsi, M.; Althueser, L.; Amaro, F.D.; Anthony, M.; Arneodo, F.; Baudis, L.; Bauermeister, B. dark matter Search Results from a One Ton-Year Exposure of XENON1T. *Phys. Rev. Lett.* **2018**, *121*, 111302. [CrossRef]
- [39] Aprile, E.; Aalbers, J.; Agostini, F.; Alfonsi, M.; Althueser, L.; Amaro, F.D.; Anthony, M.; Antochi, V.C.; Arneodo, F.; Baudis, L. Constraining the spin-dependent WIMP-nucleon cross sections with XENON1T. *Phys. Rev. Lett.* **2019**, *122*, 141301. [CrossRef]
- [40] Akerib, D.S.; Alsum, S.; Araújo, H.M.; Bai, X.; Bailey, A.J.; Balajthy, J.; Beltrame, P.; Bernard, E.P.; Bernstein, A.; Biesiadzinski, T.P.; et al. Limits on spin-dependent WIMP-nucleon cross section obtained from the complete LUX exposure. *Phys. Rev. Lett.* **2017**, *118*, 251302. [CrossRef]
- [41] Cui, X.; Abdukerim, A.; Chen, W.; Chen, X.; Chen, Y.; Dong, B.; Fang, D.; Fu, C.; Giboni, K.; Giuliani, F.; et al. dark matter Results From 54-Ton-Day Exposure of PandaX-II Experiment.

- Phys. Rev. Lett.* **2017**, *119*, 181302. [CrossRef]
- [42] Wang, W.; Wu, K.-Y.; Wu, L.; Zhu, B. Direct detection of spin-dependent sub-GeV dark matter via Migdal effect. *Nucl. Phys. B* **2022**, *983*, 115907. [CrossRef]
- [43] Wang, W.; Wu, L.; Yang, W.-N.; Zhu, B. The Spin-dependent Scattering of Boosted dark matter. *arXiv* **2021**, arXiv:2111.04000.
- [44] Shang, L.; Sun, P.; Heng, Z.; He, Y.; Yang, B. Mass-degenerate Higgs bosons near 125 GeV in the NMSSM under current experimental constraints. *Eur. Phys. J. C* **2020**, *80*, 574. [CrossRef]
- [45] Kozaczuk, J.; Profumo, S.; Haskins, L.S.; Wainwright, C.L. Cosmological Phase Transitions and their Properties in the NMSSM. *JHEP* **2015**, *1*, 144. [CrossRef]
- [46] Kozaczuk, J.; Profumo, S.; Wainwright, C.L. Electroweak Baryogenesis And The Fermi Gamma-Ray Line. *Phys. Rev. D* **2013**, *87*, 075011. [CrossRef]
- [47] Miller, D.J.; Nevzorov, R.; Zerwas, P.M. The Higgs sector of the next-to-minimal supersymmetric standard model. *Nucl. Phys. B* **2004**, *681*, 3–30. [CrossRef]
- [48] King, S.F.; Mühlleitner, M.; Nevzorov, R.; Walz, K. Natural NMSSM Higgs Bosons. *Nucl. Phys. B* **2013**, *870*, 323–352. [CrossRef]
- [49] Jeong, K.S.; Shoji, Y.; Yamaguchi, M. Singlet-Doublet Higgs Mixing and Its Implications on the Higgs mass in the PQ-NMSSM. *JHEP* **2012**, *9*, 7. [CrossRef]
- [50] Badziak, M.; Olechowski, M.; Pokorski, S. New Regions in the NMSSM with a 125 GeV Higgs. *JHEP* **2013**, *6*, 43. [CrossRef]
- [51] Aad, G.; Abbott, B.; Abdallah, J.; Abeloos, B.; Aben, R.; AbouZeid, O.S.; Abraham, N.L.; Abramowicz, H.; Abreu, H.; Abreu, R.; et al. Measurements of the Higgs boson production and decay rates and constraints on its couplings from a combined ATLAS and CMS analysis of the LHC pp collision data at $\sqrt{s} = 7$ and 8 TeV. *JHEP* **2016**, *2016*, 45. [CrossRef]
- [52] Aad, G.; Abbott, B.; Abdallah, J.; Abidinov, O.; Aben, R.; Abolins, M.; AbouZeid, O.S.; Abramowicz, H.; Abreu, H.; Abreu, R.; et al. Study of the spin and parity of the Higgs boson in diboson decays with the ATLAS detector. *Eur. Phys. J. C* **2015**, *75*, 476; Erratum in *Eur. Phys. J. C* **2016**, *76*, 152. [CrossRef]
- [53] Sirunyan, A.M.; Tumasyan, A.; Adam, W.; Ambroggi, F.; Asilar, E.; Bergauer, T.; Brandstetter, J.; Dragicevic, M.; Erö, J.; Del Valle, A.E.; et al. Combined measurements of Higgs boson couplings in proton–proton collisions at $\sqrt{s} = 13$ TeV. *Eur. Phys. J. C* **2019**, *79*, 421.

[CrossRef]

- [54] Aad, G.; Abbott, B.; Abbott, D.C.; Abud, A.A.; Abeling, K.; Abhayasinghe, D.K.; Abidi, S.H.; AbouZeid, O.S.; Abraham, N.L.; Abramowicz, H.; et al. Combined measurements of Higgs boson production and decay using up to 80 fb⁻¹ of proton-proton collision data at $\sqrt{s} = 13$ TeV collected with the ATLAS experiment. *Phys. Rev. D* **2020**, *101*, 012002. [CrossRef]
- [55] Aad, G.; Abbott, B.; Abbott, D.C.; Abud, A.A.; Abeling, K.; Abhayasinghe, D.K.; Abidi, S.H.; AbouZeid, O.S.; Abraham, N.L.; Abramowicz, H.; et al. Test of CP invariance in vector-boson fusion production of the Higgs boson in the $H \rightarrow \tau\tau$ channel in proton-proton collisions at $\sqrt{s}=13$ TeV with the ATLAS detector. *Phys. Lett. B* **2020**, *805*, 135426. [CrossRef]
- [56] Ellwanger, U.; Gunion, J.F.; Hugonie, C. NMHDECAY: A Fortran code for the Higgs masses, couplings and decay widths in the NMSSM. *JHEP* **2005**, *2*, 66. [CrossRef]
- [57] Ellwanger, U.; Hugonie, C. NMHDECAY 2.0: An Updated program for sparticle masses, Higgs masses, couplings and decay widths in the NMSSM. *Comput. Phys. Commun.* **2006**, *175*, 290–303. [CrossRef]
- [58] Bechtle, P.; Heinemeyer, S.; Stål, O.; Stefaniak, T.; Weiglein, G. *HiggsSignals*: Confronting arbitrary Higgs sectors with measurements at the Tevatron and the LHC. *Eur. Phys. J. C* **2014**, *74*, 2711. [CrossRef]
- [59] Bechtle, P.; Heinemeyer, S.; Stål, O.; Stefaniak, T.; Weiglein, G. Probing the Standard Model with Higgs signal rates from the Tevatron, the LHC and a future ILC. *JHEP* **2014**, *11*, 39. [CrossRef]
- [60] Stål, O.; Stefaniak, T. Constraining extended Higgs sectors with HiggsSignals. In Proceedings of the 2013 European Physical Society Conference on High Energy Physics (EPS-HEP 2013), Stockholm, Sweden, 18–24 July 2013.
- [61] Bechtle, P.; Brein, O.; Heinemeyer, S.; Weiglein, G.; Williams, K.E. HiggsBounds: Confronting Arbitrary Higgs Sectors with Exclusion Bounds from LEP and the Tevatron. *Comput. Phys. Commun.* **2010**, *181*, 138–167. [CrossRef]
- [62] Bechtle, P.; Brein, O.; Heinemeyer, S.; Weiglein, G.; Williams, K.E. HiggsBounds 2.0.0: Confronting Neutral and Charged Higgs Sector Predictions with Exclusion Bounds from LEP and the Tevatron. *Comput. Phys. Commun.* **2011**, *182*, 2605–2631. [CrossRef]
- [63] Belanger, G.; Boudjema, F.; Pukhov, A.; Semenov, A. dark matter direct detection rate in a generic model with micrOMEGAs 2.2. *Comput. Phys. Commun.* **2009**, *180*, 747–767.

[CrossRef]

- [64] Belanger, G.; Boudjema, F.; Brun, P.; Pukhov, A.; Rosier-Lees, S.; Salati, P.; Semenov, A. Indirect search for dark matter with micrOMEGAs2.4. *Comput. Phys. Commun.* **2011**, *182*, 842–856. [CrossRef]
- [65] Preskill, J.; Wise, M.B.; Wilczek, F. Cosmology of the Invisible Axion. *Phys. Lett. B* **1983**, *120*, 127–132. [CrossRef]
- [66] Ellis, J.R.; Hagelin, J.S.; Nanopoulos, D.V.; Olive, K.A.; Srednicki, M. Supersymmetric Relics from the Big Bang. *Nucl. Phys. B* **1984**, *238*, 453–476. [CrossRef]
- [67] Tanabashi, M.; Tanabashi, M.; Hagiwara, K.; Hikasa, K.; Nakamura, K.; Sumino, Y.; Taka-hashi, F.; Tanaka, J.; Agashe, K.; Aielli, G. and Amsler, et al. Review of Particle Physics. *Phys. Rev. D* **2018**, *98*, 030001. [CrossRef]
- [68] Hinshaw, G.; Larson, D.; Komatsu, E.; Spergel, D.N.; Bennett, C.; Dunkley, J.; Nolte, M.R.; Halpern, M.; Hill, R.S.; Odegard, N.; et al. Nine-Year Wilkinson Microwave Anisotropy Probe (WMAP) Observations: Cosmological Parameter Results. *Astrophys. J. Suppl.* **2013**, *208*, 19. [CrossRef]
- [69] Ade, P.A.; Aghanim, N.; Armitage-Caplan, C.; Arnaud, M.; Ashdown, M.; Atrio-Barandela, F.; Aumont, J.; Baccigalupi, C.; Banday, A.J.; Barreiro, R.B.; et al. Planck 2013 results. XVI. Cosmological parameters. *Astron. Astrophys.* **2014**, *571*, A16.
- [70] Beenakker, W.; Hopker, R.; Spira, M. PROSPINO: A Program for the production of super-symmetric particles in next-to-leading order QCD. *arXiv* **1996**, arXiv:hep-ph/9611232.
- [71] Kraml, S.; Kulkarni, S.; Laa, U.; Lessa, A.; Magerl, W.; Proschofsky-Spindler, D.; Wal-tenberger, W. SModelS: A tool for interpreting simplified-model results from the LHC and its application to supersymmetry. *Eur. Phys. J. C* **2014**, *74*, 2868. [CrossRef]